

Spin Crossover

International Edition: DOI: 10.1002/anie.201914343
German Edition: DOI: 10.1002/ange.201914343

Confined Crystallization of Spin-Crossover Nanoparticles in Block-Copolymer Micelles

Christoph Göbel, Christian Hils, Markus Drechsler, Dirk Baabe, Andreas Greiner, Holger Schmalz,* and Birgit Weber*

Abstract: Nanoparticles of the spin-crossover coordination polymer $[\text{FeL}(\text{bipy})]_n$ were synthesized by confined crystallization within the core of polystyrene-block-poly(4-vinylpyridine) (PS-*b*-P4VP) diblock copolymer micelles. The 4VP units in the micellar core act as coordination sites for the Fe complex. In the bulk material, the spin-crossover nanoparticles in the core are well isolated from each other allowing thermal treatment without disintegration of their structure. During annealing above the glass transition temperature of the PS block, the transition temperature is shifted gradually to higher temperatures from the as-synthesized product ($T_{1/2\downarrow} = 163\text{ K}$ and $T_{1/2\uparrow} = 170\text{ K}$) to the annealed product ($T_{1/2\downarrow} = 203\text{ K}$ and $T_{1/2\uparrow} = 217\text{ K}$) along with an increase in hysteresis width from 6 K to 14 K. Thus, the spin-crossover properties can be shifted towards the properties of the related bulk material. The stability of the nanocomposite allows further processing, such as electrospinning from solution.

Introduction

The synthesis of nanoparticles (NPs) of functional materials is often considered an important step towards application.^[1] A highly relevant aspect to consider is the stability of the obtained NPs, the conservation of their functional properties down to very small sizes (if possible the observation of additional size-dependent properties) and the suitability for integration into devices. The spin crossover (SCO) phenomenon has gained interest in many different fields over the last decades.^[2–6] SCO complexes can be switched between two states, the high-spin (HS) and the low-spin (LS) state, by a wide range of external stimuli^[7] such as temperature,

pressure, light irradiation or the inclusion of guest molecules.^[4,8] Furthermore, the physical properties of either the complex itself (e.g. color, magnetism, structure)^[5,9] or associated properties in multifunctional systems (e.g. conductivity,^[10] luminescence^[11]) change upon switching and raise their interest for applications, especially as sensors.^[12] In order to realize such applications, an easy processing of the complexes is indispensable for the integration in devices. This task (including down-sizing) is challenging as most of the SCO properties, especially the observation of wide thermal hysteresis loops, depend on the crystal packing.^[6] So far, to our knowledge, only five examples are known in which thermal hysteresis loops can be maintained for particle sizes below 20 nm.^[13–16] In general, SCO systems are excellently suited to investigate the influence of decreasing particle size,^[15,17–19] crystallinity and matrix effects^[16,20–22] on the nanomaterial as a wide range of different methods can be used to follow the SCO. Those investigations lead to the observation of different phenomena like the predicted re-appearance of hysteresis loops below a 8 nm particle size^[18] or the stabilizing effect of a rigid SiO₂ shell on the hysteresis for 10 nm^[16] particles as well as larger ones.^[22]

In a prior work, we reported a new approach for the synthesis of narrowly distributed 50 nm SCO nanoparticles within the P4VP cores of PS-*b*-P4VP block copolymer (BCP) micelles, where a shift of the SCO transition temperature to lower temperatures and a significantly smaller thermal hysteresis loop was observed.^[23,24] Herein, we show that it is possible to trigger the crystallization of even smaller nanoparticles in the micellar confinement, if the material is heated above the glass transition temperature of the PS shell. This

[*] C. Göbel, Prof. Dr. B. Weber
Department of Chemistry
Inorganic Chemistry IV, Universität Bayreuth
Universitätsstrasse 30, 95440 Bayreuth (Germany)
E-mail: weber@uni-bayreuth.de

C. Hils
Department of Chemistry, Macromolecular Chemistry II, Universität Bayreuth
Universitätsstr. 30, 95440 Bayreuth (Germany)

Prof. Dr. A. Greiner, Dr. H. Schmalz
Department of Chemistry, Macromolecular Chemistry II and Keylab Synthesis and Molecular Characterization, Bavarian Polymer Institute, Universität Bayreuth
Universitätsstrasse 30, 95440 Bayreuth (Germany)
E-mail: holger.schmalz@uni-bayreuth.de

M. Drechsler
Keylab Electron and Optical Microscopy, Bavarian Polymer Institute, Universität Bayreuth
Universitätsstrasse 30, 95440 Bayreuth (Germany)

Dr. D. Baabe
Institut für Anorganische und Analytische Chemie, Technische Universität Braunschweig
Hagenring 30, 38106 Braunschweig (Germany)

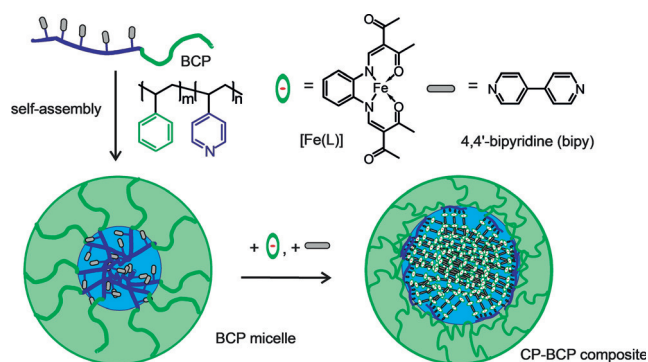
Supporting information and the ORCID identification number(s) for the author(s) of this article can be found under:
<https://doi.org/10.1002/anie.201914343>.

© 2019 The Authors. Published by Wiley-VCH Verlag GmbH & Co. KGaA. This is an open access article under the terms of the Creative Commons Attribution Non-Commercial NoDerivs License, which permits use and distribution in any medium, provided the original work is properly cited, the use is non-commercial, and no modifications or adaptations are made.

leads to a significant improvement of the SCO properties down to particle sizes as small as 16 nm.

Results and Discussion

The spin crossover coordination polymer–block copolymer (SCO CP-BCP) composite particles were synthesized as described previously by dissolving the PS-*b*-P4VP diblock copolymer ($S_{85}V_{15}^{154}$; subscripts denote content of the respective block in wt %, superscript gives the number average molecular weight in kgmol^{-1}) and the complex $[\text{FeL}(\text{MeOH})_2]$ in tetrahydrofuran (THF) followed by subsequent addition of the bridging ligand 4,4'-bipyridine (bipy) and iron complex under reflux conditions (Scheme 1, see Supporting Information for details).^[20] In total five cycles of addition of



Scheme 1. General synthesis approach and abbreviations used.

complex and bridging ligand were carried out, leading to a ratio of about 33.5 mg of iron complex in 50 mg BCP. Raman measurements on the produced SCO CP-BCP composite particles revealed identical Raman spectra compared to that observed for the neat SCO CP crystals, confirming the successful formation of SCO CP in the micellar core of the $S_{85}V_{15}^{154}$ micelles (Figure S1 in the Supporting Information); also confirmed by IR spectroscopy (Figure S2). The average hydrodynamic diameter of the SCO CP-BCP particles in solution was determined to $D_h = 87 \pm 37$ nm (Figure 1E, for corresponding autocorrelation function see Figure S3) by dynamic light scattering (DLS), which is slightly larger compared to that of the empty BCP micelles ($D_h = 75 \pm 28$ nm, Figure 1C and Figure S3). This might be attributed to the incorporation of the SCO CP inside the P4VP core of the micelle. The different sizes are also reflected in the cryo-TEM pictures for the empty BCP micelles (Figure 1A) and the SCO CP-BCP particles (Figure 1D). Cryo-TEM confirms the spherical shape of both the empty BCP micelle cores with a size of 26 ± 2 nm (Figure 1C) as well as the composite nanoparticles with a size of 34 ± 5 nm (Figure 1F).

TEM measurements of the SCO CP-BCP composite particles in the dry state, clearly reveal the core-shell structure of the particles, with the dark appearing domains corresponding to the P4VP core containing the iron CP and the grey appearing domains to the PS block forming the shell

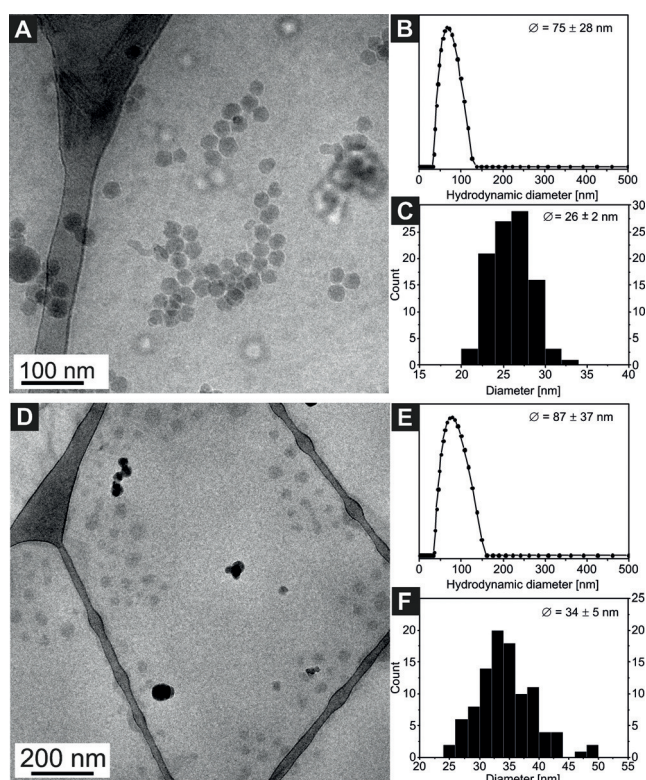


Figure 1. Cryo-TEM image of the narrowly dispersed spherical BCP micelles (A) with the hydrodynamic diameter distribution determined by DLS (B) and the size distribution derived from the image (C). Cryo-TEM image of the narrowly dispersed spherical SCO CP-BCP particles (D) with the hydrodynamic diameter distribution determined by DLS (E) and the size distribution derived from the image (F). (Corresponding DLS autocorrelation functions of both samples can be found in Figure S3.)

(Figure 2C). For the size distribution of the particles only the core of the particles was measured and a core diameter of $D_{\text{core}} = 16 \pm 2$ nm is obtained (Figure 2E), while the empty BCP micelle cores have a diameter of $D_{\text{core}} = 15 \pm 2$ nm (Figure 2B). The coordination of the paramagnetic complex $[\text{FeL}]$ to the P4VP units is also confirmed by the paramagnetic shift of the 4VP signals in the $^1\text{H NMR}$ spectrum of the nanocomposite (Figure S11) compared to the pure BCP.

The magnetic properties of the SCO CP-BCP composite particles were analyzed using temperature-dependent magnetic measurements and Mössbauer spectroscopy. The room temperature Mössbauer spectrum of the composite allows to identify the different iron species that may occur during the synthesis and is given in Figure S4.^[20] It shows one distinct doublet that can be attributed to a Fe^{II} HS species. The doublet has an isomer shift δ of $0.937(6)$ mm s^{-1} , a quadrupole splitting ΔE_Q of $2.177(13)$ mm s^{-1} and a line width (HWHM) of $0.193(10)$ mm s^{-1} that is characteristic for the CP $[\text{FeL}(\text{bipy})]_n$.^[23]

Figure 3 shows the $\chi_M T$ vs. T plot for the sample measured in sweep and settle mode to investigate the effect of the BCP confinement and thermal annealing on the SCO properties of the CP. Different cooling and heating cycles were performed to trace the change of the spin transition regarding final $\chi_M T$

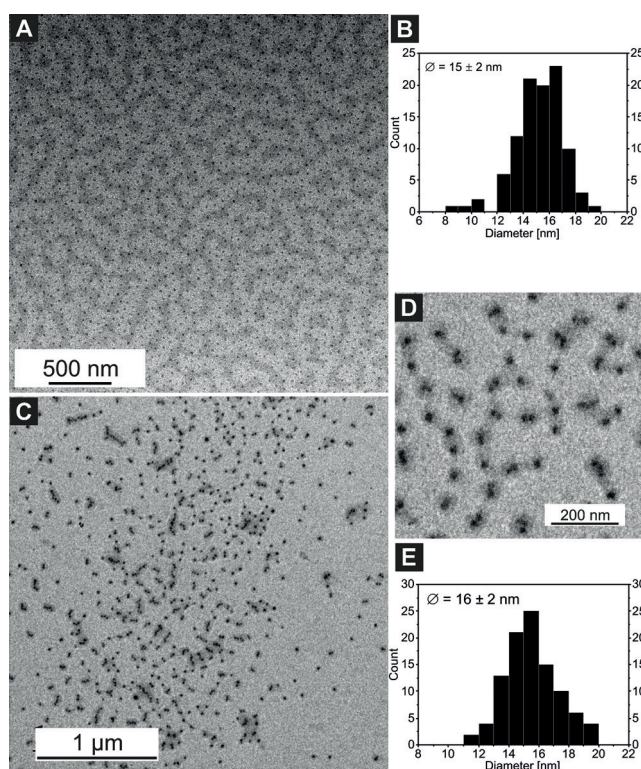


Figure 2. TEM image of the empty BCP micelles (A) with size distribution of the P4VP cores (B). TEM image of the narrowly dispersed SCO CP-BCP particles at low (C) and high (D) magnifications with size distribution of the SCO CP-BCP composite cores (E).

values, transition temperature and hysteresis width. A pure Fe^{II} HS compound of the used CP typically has a $\chi_M T$ value of around $3.25 \text{ cm}^3 \text{ K mol}^{-1}$ at 300 K. Since the Mössbauer spectrum shows that the compound is a pure HS Fe^{II} species, the starting value of the as-synthesized product is adjusted to $3.25 \text{ cm}^3 \text{ K mol}^{-1}$ at 300 K. All information on cooling and heating cycles performed on the SCO CP-BCP are summarized in Table 1. Upon cycle 1 (black curve, Figure 3 A) down to 50 K the $\chi_M T$ value stays approximately constant down to 200 K, where a rather gradual spin transition takes place with $T_{1/2\downarrow} = 163 \text{ K}$. The $\chi_M T$ value drops to $1.70 \text{ cm}^3 \text{ K mol}^{-1}$ at 50 K leaving around 52 % of the Fe^{II} centers in the HS state. Heating to 370 K reveals a 7 K wide hysteresis with $T_{1/2\uparrow} = 170 \text{ K}$. With cycles 2 to 5 the transition temperatures are shifted to higher temperatures, reaching $T_{1/2\downarrow} = 200 \text{ K}$ and $T_{1/2\uparrow} = 217 \text{ K}$, while also lowering the $\chi_M T$ values at 50 K down to $1.27 \text{ cm}^3 \text{ K mol}^{-1}$ after cycle 5 (Table 1). Thus, the SCO is more complete after the annealing process revealing a molar fraction of high-spin molecules of $\gamma_{\text{HS}} = 0.39$. Although the CP is confined inside the micellar core, the hysteresis width of the SCO CP-BCP particles of 17 K is similar to the one of the bulk material (18 K). However, it is already known that a higher

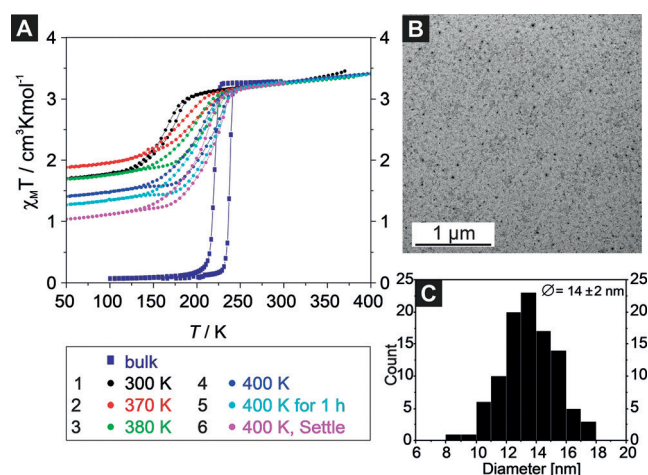


Figure 3. Magnetic susceptibility data for the SCO CP-BCP composite particles given as $\chi_M T$ vs. T plot measured in sweep and settle mode (A). The colors represent different cooling and heating cycles as stated in the bottom left corner. For comparison, the results for the bulk material^[25] are included as well. TEM image of the SCO CO-BCP particles after annealing showing no agglomeration or enlargement of the particles (B). Size distribution of the particles derived from the given TEM image (C).

scan rate can lead to kinetic effects that broaden the hysteresis width.^[6,26] These effects can be eliminated by using the settle mode because the effective scan rate is reduced, giving the system time to adapt to the changed temperature. Therefore, the final cooling and heating cycle 6 from 400 K to 50 K and back to 300 K is performed in settle mode to show that the change induced by the thermal treatment is persistent and the hysteresis is smaller in the composite particles (Figure 3 A, pink). In fact, the transition is even more complete than the one measured in sweep mode with a $\chi_M T$ value of $1.04 \text{ cm}^3 \text{ K mol}^{-1}$ at 50 K ($\gamma_{\text{HS}} = 0.32$). This is in good agreement with the expected HS fraction of $\gamma_{\text{HS}} = 0.22$ for spherical 16 nm particles assuming that each iron center and the surrounding ligand occupies the space of 1 nm^3 . The hysteresis width is narrowed to 14 K with $T_{1/2\downarrow} = 203 \text{ K}$ and $T_{1/2\uparrow} = 217 \text{ K}$ (Table 1). Temperature-dependent Mössbauer spectra were used to confirm the results from the magnetic measurements, the results are summarized in Table 2 and Table S1 and in Figure S12. Please note that due to the long measurement times only settle measurements are possible

Table 1: Data of the magnetic measurements for the different heating cycles. The measurement modes, transition temperatures, hysteresis widths and $\chi_M T$ values are given. The sweep rate is 5 K min^{-1} .

Entry	Heating cycle [K]	Mode	$T_{1/2\downarrow}$ [K]	$T_{1/2\uparrow}$ [K]	Hysteresis width [K]	$\chi_M T$ at 50 K [$\text{cm}^3 \text{ K mol}^{-1}$]
1	300–50–370 ^[a]	sweep	163	170	7	1.70
2	370–50–380 ^[b]	sweep	179	192	13	1.88
3	380–50–400 ^[c]	sweep	192	207	15	1.69
4	400–50–400 ^[d]	sweep	198	215	17	1.40
5	400–50–300 ^[e]	sweep	200	217	17	1.27
6	400–50–300 ^[f]	settle	203	217	14	1.04

[a] Figure 3 A, curve 1. [b] Figure 3 A, curve 2. [c] Figure 3 A, curve 3. [d] Figure 3 A, curve 4. [e] Figure 3 A, curve 5. [f] Figure 3 A curve 6.

and the thermal annealing was done at 393 K for 1 h leading to HS fractions more comparable to curve 3 or 4 in Figure 3 (see Table 2). Thermogravimetric analysis (TGA) of the sample before the annealing process shows no significant mass loss (relative loss around 0.1 % until 100 °C, Figure S5). This indicates that a loss of residual solvent cannot be responsible for the improved SCO behavior.

Table 2: The molar fraction of high-spin molecules (γ_{HS}) determined by Mössbauer spectroscopy (see Table S1) and magnetic susceptibility measurements (see Figure 3).

T [K]	$\gamma_{\text{HS}}^{[a]}$	$\gamma_{\text{HS}}^{[b]}$	$\gamma_{\text{HS}}^{[c]}$	$\gamma_{\text{HS}}^{[d]}$	$\gamma_{\text{HS}}^{[e]}$
175 ^[f]	0.80	0.86	0.68	0.63	0.58
80	0.62	0.62	0.54	0.55	0.45
175 ^[g]	0.74	0.80	0.61	0.58	0.50

[a],[d] Values determined by Mössbauer spectroscopy before and after annealing, respectively. [b],[c],[e] Values determined by magnetic susceptibility measurements (Figure 3, curves “1”, “3”, and “4”, respectively). [f] Data recorded upon cooling. [g] Data recorded upon heating.

Moreover, the improved SCO behavior is also not a result of the formation of microcrystals or agglomerated particles due to the exposure to elevated temperatures as indicated by TEM and DLS measurements on the redispersed SCO CP-BCP particles taken after the magnetic measurement (Figure 3 B and Figure S6). The TEM measurement of the sample after thermal annealing shows particles of similar size and shape compared to the ones before annealing with core sizes of 14 ± 2 nm (Figure 3 C). Consequently, DLS underlines that the composite particles are still intact after annealing with an average D_h of 106 ± 67 nm (Figure S6). Further proof is given by SEM measurements that were performed before and after the annealing (Figure S7). No formation of microcrystals ($>1 \mu\text{m}$) or larger nanoparticles was observed. SEM-EDX measurements show that the iron is homogeneously distributed throughout the sample.

Temperature-dependent powder X-ray diffraction (PXRD) was measured to follow any change in the crystallinity of the sample caused by the annealing process (Figure 4). The sample was heated stepwise from RT to 333 K, 373 K, and 398 K and then cooled down back to RT to follow a possible change on the diffraction pattern induced by the temperature increase and to show that the changes are persistent after the annealing process. It was found that new reflexes appear at $9.6^\circ 2\theta$ and $15.4^\circ 2\theta$ not before 373 K and remain when the sample was cooled down to RT. In contrast, a reflex at $25.8^\circ 2\theta$ disappears at 373 K and above and remains absent back at RT. This led to the conclusion that some sort of reorientation occurs inside the SCO CP-BCP composite particles at temperatures above the glass transition temperature of the PS ($T_g(\text{PS}) = 383$ K, Figure S9). After heating, the diffraction pattern shows more similarity with the one of the bulk material.

The results indicate that by thermal treatment, especially when the composite particles are heated to and above T_g of the PS shell of 383 K, the crystallinity of the SCO CP inside the micellar core is improved because the PS chains become

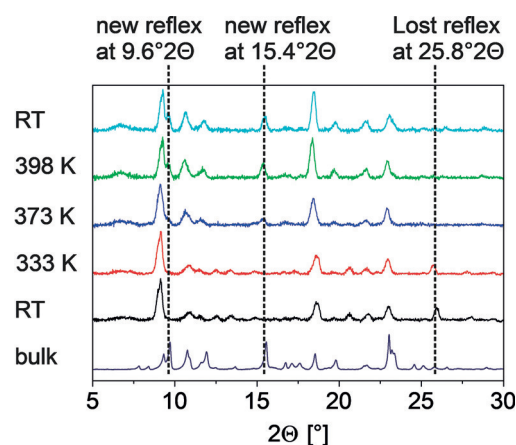


Figure 4. Temperature-dependent powder X-ray diffraction of the SCO CP-BCP composite particles.

flexible, allowing the SCO CP to reorder inside the polymeric micelle.

The synthesized SCO CP-BCP particles can be used to prepare PS/SCO CP composite fibers by electrospinning, a widely used technique employed for the production of polymer fibers of various shapes and properties.^[27] Figure 5 A shows PS/SCO CP composite fibers, which were spun from a mixture of PS ($M_n = 97\,000$ g mol⁻¹, $D = 1.02$) and SCO CP-BCP particles in THF on aluminum foil (details on electrospinning can be found in the SI). The obtained color is typical for iron complexes of this ligand type, however, probably due to the remaining HS fraction, no significant color change upon cooling was observed. The presence of the SCO

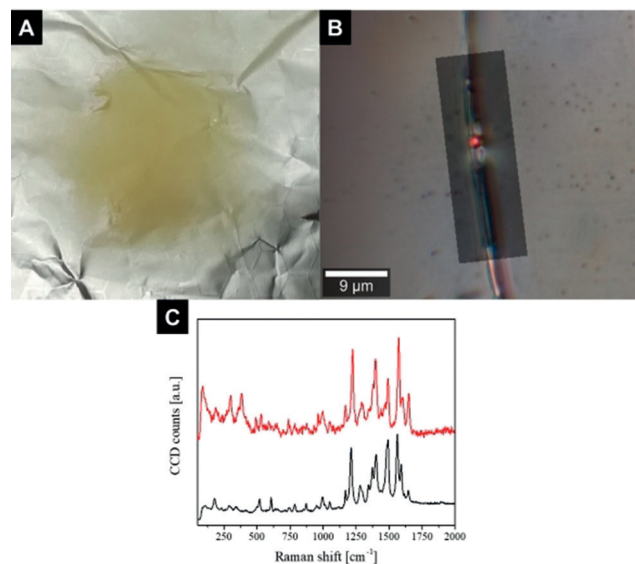


Figure 5. Digital photograph of electrospun PS/SCO CP composite fibers on aluminum foil (A), digital photograph of a single fiber overlaid with the color-coded 2D Raman image (B) and corresponding Raman spectra (C) of the SCO CP in the BCP micelles (black) and in PS fibers (red). As the SCO CP crystals in the micellar core are strong Raman scatterers, Raman imaging with a very low laser intensity of 0.1 mW allows a selective detection of the SCO CP particles in the composite fibers. Under these conditions PS shows no Raman signal.

complex particles in the fibers was confirmed by Raman imaging (Figure 5B, C). A very low laser power of 0.1 mW was employed, where only the SCO complex shows a Raman signal and, thus, a selective detection of the SCO complex in the composite fibers is possible. The overlay of the digital photograph with the Raman image clearly confirms the presence of the SCO complex (colored in red, Figure 5B) in the fibers. Moreover, the Raman spectra of the SCO complex in the neat SCO CP-BCP particles and in the composite fibers are identical, showing that electrospinning does not alter the structure of the SCO complex.

Conclusion

In conclusion, we have shown that the transition temperature of the SCO CP-BCP $[\text{FeL}(\text{bipy})]_n$ can be shifted gradually by thermal annealing. Starting with the as-synthesized product and the transition temperatures $T_{1/2\downarrow}$ and $T_{1/2\uparrow}$ of 163 K and 170 K respectively, the transition temperature is shifted 40 K to higher temperatures to reach its final state after several annealing steps with $T_{1/2\downarrow} = 203$ K and $T_{1/2\uparrow} = 217$ K. Furthermore, the hysteresis width is also broadened by the annealing process from 6 K (sweep) for the as-synthesized product to 17 K (sweep) for the annealed product. The subsequent susceptibility measurement in settle mode showed that the change in the transition temperature is persistent with a hysteresis width of 14 K and an improved completeness of the spin transition from $\gamma_{\text{HS}} = 0.52$ to $\gamma_{\text{HS}} = 0.32$. Magnetic susceptibility, TGA and temperature-dependent PXRD data support the assumption that the transition temperature change is a consequence of the thermal annealing and recrystallization instead of a solvent loss of the sample or particle agglomeration. The demonstrated approach is potentially applicable to other polymeric SCO systems and offers an approach to fine-tune the transition temperatures by different polymer shells. It will be especially interesting to explore other linear polymers, such as the triazole-based systems that, with the methods used so far, often show stable hysteresis loops down to very small particle sizes.^[13,19,20,22,28] The question arises if the different NP synthesis approaches (interaction with the polymer shell vs. surfactant) or differences in the SCO complexes (steric demand of the ligands, intermolecular interactions responsible of the observation of the hysteresis) are relevant factors. With regard to the relatively high remaining HS fraction observed, this can be clearly denoted to the ligand system, with the more bulky Schiff base-like ligands compared to the triazoles leading to a higher fraction of complexes on the surface not undergoing SCO. Thus, an increase in particle size should lead to a reduction of the remaining HS fraction. With the still relatively limited data available, the other questions can so far not be answered satisfactorily and are still under investigation. Furthermore the SCO CP-BCP composite particles are suitable for polymer processing techniques, such as electrospinning, employing a mixture with PS as fiber-forming matrix.

Acknowledgements

Financial support of the University of Bayreuth and the SFB 840 (TP A10 and A2) is gratefully acknowledged. C.G. and C.H. were supported by the BayNAT program of the University of Bayreuth graduate school. We thank Dr. Jana Timm and Prof. Dr. Roland Marschall (Physikalische Chemie III, UBT) for their contribution to the temperature-dependent PXRD measurement and Dr. Wolfgang Milius (Anorganische Chemie I, UBT) for the measurement itself. We also thank Rika Schneider (Makromolekulare Chemie II, UBT) for DSC, GPC and NMR measurements of the BCP, Marco Schwarzmann (Anorganische Chemie I, UBT) for TGA and Dr. Christine Denner (Anorganische Chemie II, UBT) for SEM and SEM-EDX measurements. D.B. thanks Prof. Dr. F. J. Litterst (Institut für Physik der Kondensierten Materie) at TU Braunschweig for providing access to the ^{57}Fe Mössbauer spectrometer.

Conflict of interest

The authors declare no conflict of interest.

Keywords: block copolymers · composite materials · electrospinning · nanoparticles · spin crossover

How to cite: *Angew. Chem. Int. Ed.* **2020**, *59*, 5765–5770
Angew. Chem. **2020**, *132*, 5814–5819

- [1] a) E. Coronado, *Nat. Rev. Mater.* **2019**, *24*, 834; b) K. Senthil Kumar, M. Ruben, *Coord. Chem. Rev.* **2017**, *346*, 176; c) K. Otsubo, T. Haraguchi, H. Kitagawa, *Coord. Chem. Rev.* **2017**, *346*, 123; d) P. N. Martinho, C. Rajnak, M. Ruben in *Spin-Crossover Materials* (Ed.: M. A. Halcrow), Wiley, Chichester, **2013**, pp. 375–404; e) M. Sindoro, N. Yanai, A.-Y. Jee, S. Granick, *Acc. Chem. Res.* **2014**, *47*, 459; f) E. A. Flügel, A. Ranft, F. Haase, B. V. Lotsch, *J. Mater. Chem.* **2012**, *22*, 10119.
- [2] a) M.-L. Boillot, B. Weber, *C. R. Chim.* **2018**, *21*, 1196; b) P. G. Lacroix, I. Malfant, C. Lepetit, *Coord. Chem. Rev.* **2016**, *308*, 381; c) A. B. Gaspar, M. Seredyuk, *Coord. Chem. Rev.* **2014**, *268*, 41; d) *Spin-Crossover Materials* (Ed.: M. A. Halcrow), Wiley, Chichester, **2013**; e) D. J. Harding in *Advanced Nanomaterials* (Eds.: E. Rentschler, N. Domracheva, M. Caporali), Elsevier, Amsterdam, **2018**, pp. 401–426.
- [3] A. B. Gaspar, B. Weber in *Molecular Magnetic Materials* (Eds.: B. Sieklucka, D. Pinkowicz), Wiley-VCH, Weinheim, **2017**, pp. 231–252.
- [4] Z.-P. Ni, J.-L. Liu, M. N. Hoque, W. Liu, J.-Y. Li, Y.-C. Chen, M.-L. Tong, *Coord. Chem. Rev.* **2017**, *335*, 28.
- [5] D. J. Harding, P. Harding, W. Phonsri, *Coord. Chem. Rev.* **2016**, *313*, 38.
- [6] S. Brooker, *Chem. Soc. Rev.* **2015**, *44*, 2880.
- [7] a) P. Gütllich, A. Hauser, H. Spiering, *Angew. Chem. Int. Ed. Engl.* **1994**, *33*, 2024; *Angew. Chem.* **1994**, *106*, 2109; b) *Topics in Current Chemistry, Vol. 233–235* (Eds.: P. Gütllich, H. A. Goodwin), Springer Berlin/Heidelberg, Berlin, **2004**.
- [8] a) E. Coronado, M. Giménez-Marqués, G. Mínguez Espallargas, F. Rey, I. J. Vitórica-Yrezábal, *J. Am. Chem. Soc.* **2013**, *135*, 15986; b) M. Ohba, K. Yoneda, G. Agustí, M. C. Muñoz, A. B. Gaspar, J. A. Real, M. Yamasaki, H. Ando, Y. Nakao, S. Sakaki,

- et al., *Angew. Chem. Int. Ed.* **2009**, *48*, 4767; *Angew. Chem.* **2009**, *121*, 4861; c) P. D. Southon, L. Liu, E. A. Fellows, D. J. Price, G. J. Halder, K. W. Chapman, B. Moubarak, K. S. Murray, J.-F. Létard, C. J. Kepert, *J. Am. Chem. Soc.* **2009**, *131*, 10998.
- [9] a) F. J. Valverde-Muñoz, M. C. Muñoz, S. Ferrer, C. Bartual-Murgui, J. A. Real, *Inorg. Chem.* **2018**, *57*, 12195; b) M. Attwood, H. Akutsu, L. Martin, D. Cruickshank, S. S. Turner, *Dalton Trans.* **2019**, *48*, 90; c) E. Collet, P. Guionneau, *C. R. Chim.* **2018**, *21*, 1133.
- [10] a) H.-Y. Wang, J.-Y. Ge, C. Hua, C.-Q. Jiao, Y. Wu, C. F. Leong, D. M. D'Alessandro, T. Liu, J.-L. Zuo, *Angew. Chem. Int. Ed.* **2017**, *56*, 5465; *Angew. Chem.* **2017**, *129*, 5557; b) Y.-C. Chen, Y. Meng, Z.-P. Ni, M.-L. Tong, *J. Mater. Chem. C* **2015**, *3*, 945; c) Y.-S. Koo, J. R. Galán-Mascarós, *Adv. Mater.* **2014**, *26*, 6785; d) T. G. Gopakumar, F. Matino, H. Naggert, A. Bannwarth, F. Tuzcek, R. Berndt, *Angew. Chem. Int. Ed.* **2012**, *51*, 6262; *Angew. Chem.* **2012**, *124*, 6367.
- [11] a) C. Lochenie, K. Schötz, F. Panzer, H. Kurz, B. Maier, F. Puchtler, S. Agarwal, A. Köhler, B. Weber, *J. Am. Chem. Soc.* **2018**, *140*, 700; b) B. Schäfer, T. Bauer, I. Faus, J. A. Wolny, F. Dahms, O. Fuhr, S. Lebedkin, H.-C. Wille, K. Schlage, K. Chevalier, et al., *Dalton Trans.* **2017**, *46*, 2289; c) I. Suleimanov, O. Kraieva, J. Sánchez Costa, I. O. Fritsky, G. Molnár, L. Salmon, A. Bousseksou, *J. Mater. Chem. C* **2015**, *3*, 5026; d) C.-F. Wang, R.-F. Li, X.-Y. Chen, R.-J. Wei, L.-S. Zheng, J. Tao, *Angew. Chem. Int. Ed.* **2015**, *54*, 1574; *Angew. Chem.* **2015**, *127*, 1594; e) I. Suleimanov, O. Kraieva, G. Molnár, L. Salmon, A. Bousseksou, *Chem. Commun.* **2015**, *51*, 15098.
- [12] a) R. G. Miller, S. Brooker, *Chem. Sci.* **2016**, *7*, 2501; b) O. Kraieva, C. M. Quintero, I. Suleimanov, E. M. Hernandez, D. Lagrange, L. Salmon, W. Nicolazzi, G. Molnar, C. Bergaud, A. Bousseksou, *Small* **2016**, *12*, 6325; c) J. Huang, R. Xie, W. Wang, Q. Li, J. Yang, *Nanoscale* **2016**, *8*, 609; d) J. Dugay, M. Aarts, M. Giménez-Marqués, T. Kozlova, H. W. Zandbergen, E. Coronado, H. S. J. van der Zant, *Nano Lett.* **2017**, *17*, 186; e) M. Bernien, H. Naggert, L. M. Arruda, L. Kipgen, F. Nickel, J. Miguel, C. F. Hermanns, A. Krüger, D. Krüger, E. Schierle, et al., *ACS Nano* **2015**, *9*, 8960; f) G. Molnár, L. Salmon, W. Nicolazzi, F. Terki, A. Bousseksou, *J. Mater. Chem. C* **2014**, *2*, 1360; g) L. Salmon, L. Catala, *C. R. Chim.* **2018**, *21*, 1230.
- [13] E. Coronado, J. R. Galán-Mascarós, M. Monrabal-Capilla, J. García-Martínez, P. Pardo-Ibáñez, *Adv. Mater.* **2007**, *19*, 1359.
- [14] a) H. Peng, S. Tricard, G. Félix, G. Molnár, W. Nicolazzi, L. Salmon, A. Bousseksou, *Angew. Chem. Int. Ed.* **2014**, *53*, 10894; *Angew. Chem.* **2014**, *126*, 11074; b) F. Volatron, L. Catala, E. Rivière, A. Gloter, O. Stéphan, T. Mallah, *Inorg. Chem.* **2008**, *47*, 6584.
- [15] J. R. Galán-Mascarós, E. Coronado, A. Forment-Aliaga, M. Monrabal-Capilla, E. Pinilla-Cienfuegos, M. Ceolin, *Inorg. Chem.* **2010**, *49*, 5706.
- [16] Y. Raza, F. Volatron, S. Moldovan, O. Ersen, V. Huc, C. Martini, F. Brisset, A. Gloter, O. Stephan, A. Bousseksou, et al., *Chem. Commun.* **2011**, *47*, 11501.
- [17] M. Giménez-Marqués, M. L. García-Sanz de Larrea, E. Coronado, *J. Mater. Chem. C* **2015**, *3*, 7946.
- [18] G. Félix, W. Nicolazzi, L. Salmon, G. Molnár, M. Perrier, G. Maurin, J. Larionova, J. Long, Y. Guari, A. Bousseksou, *Phys. Rev. Lett.* **2013**, *110*, 235701.
- [19] R. Torres-Cavanillas, L. Lima-Moya, F. D. Tichelaar, H. W. Zandbergen, D. M. Giménez Marqués, E. Coronado, *ChemRxiv* **2019**, <https://doi.org/10.26434/chemrxiv.7613984.v1>.
- [20] C. Bartual-Murgui, E. Natividad, O. Roubeau, *J. Mater. Chem. C* **2015**, *3*, 7916.
- [21] D. Tanaka, N. Aketa, H. Tanaka, S. Horike, M. Fukumori, T. Tamaki, T. Inose, T. Akai, H. Toyama, O. Sakata, et al., *Dalton Trans.* **2019**, *48*, 7074.
- [22] J. M. Herrera, S. Títos-Padilla, S. J. A. Pope, I. Berlanga, F. Zamora, J. J. Delgado, K. V. Kamenev, X. Wang, A. Prescimone, E. K. Brechin, et al., *J. Mater. Chem. C* **2015**, *3*, 7819.
- [23] O. Klimm, C. Gobel, S. Rosenfeldt, F. Puchtler, N. Miyajima, K. Marquardt, M. Drechsler, J. Breu, S. Forster, B. Weber, *Nanoscale* **2016**, *8*, 19058.
- [24] a) B. Weber, *Chem. Eur. J.* **2017**, *23*, 18093; b) C. Göbel, O. Klimm, F. Puchtler, S. Rosenfeldt, S. Förster, B. Weber, *Beilstein J. Nanotechnol.* **2017**, *8*, 1318.
- [25] a) B. Weber, R. Tandon, D. Himsl, *Z. Anorg. Allg. Chem.* **2007**, *633*, 1159; b) B. Weber, E. S. Kaps, C. Desplanches, J.-F. Létard, *Eur. J. Inorg. Chem.* **2008**, 2963.
- [26] a) J. Weihermüller, S. Schlamp, B. Dittrich, B. Weber, *Inorg. Chem.* **2019**, *58*, 1278; b) S. Schönfeld, C. Lochenie, P. Thoma, B. Weber, *CrystEngComm* **2015**, *17*, 5389.
- [27] a) S. Agarwal, A. Greiner, J. H. Wendorff, *Prog. Polym. Sci.* **2013**, *38*, 963; b) A. Greiner, J. H. Wendorff, *Angew. Chem. Int. Ed.* **2007**, *46*, 5670; *Angew. Chem.* **2007**, *119*, 5770.
- [28] a) T. Forestier, S. Mornet, N. Daro, T. Nishihara, S.-i. Mouri, K. Tanaka, O. Fouche, E. Freysz, J.-F. Letard, *Chem. Commun.* **2008**, 4327; b) T. Forestier, A. Kaiba, S. Pechev, D. Denux, P. Guionneau, C. Etrillard, N. Daro, E. Freysz, J.-F. Letard, *Chem. Eur. J.* **2009**, *15*, 6122; c) A. Tokarev, L. Salmon, Y. Guari, W. Nicolazzi, G. Molnár, A. Bousseksou, *Chem. Commun.* **2010**, *46*, 8011.

Manuscript received: November 10, 2019

Accepted manuscript online: December 31, 2019

Version of record online: February 3, 2020